Journal of Constructional Steel Research 236 (2026) 109938

Contents lists available at ScienceDirect

Journal of Constructional Steel Research

journal homepage: www.elsevier.com/locate/jcsr

Behaviour of reduced web section connections in fire - an experimental and numerical study

Oday Yabari [a], Katherine A. Cashell [a,*], Mika Alanen [b], Mikko Malaska [b]

[a] University College London, Gower Street, London, UK
[b] Tampere University, P.O. Box 600, FI-33014, Finland

ARTICLE INFO

Keywords:
Steel structures
Joints
Structural response
Fire test
RWS connection

ABSTRACT

This paper presents a comprehensive investigation into the fire behaviour of steel beams with reduced web section (RWS) connections, which are commonly employed to enhance ductility in seismic design. Despite their increasing popularity in real applications in steel design for seismic regions, the performance of RWS connections under fire conditions has not been thoroughly investigated. This study details the results of the first fire test conducted on an RWS connection, carried out at the fire laboratory of Tampere University. Complementing the experimental work, a finite element model was developed and validated against the test data, allowing for an extensive parametric study. Key variables examined include steel grade, load ratio, and geometric properties of the elliptical cuts in the web. The results reveal that duplex stainless steel grade 1.477 offers the greatest fire resistance among the materials tested, while carbon steel performs the least well. Furthermore, increasing the load ratio generally reduces fire resistance, with carbon and austenitic stainless steels being particularly sensitive to this parameter. Based on these observations, design recommendations are provided to optimize the fire resistance of RWS connections.

1. Introduction

This paper is concerned with the behaviour of steel moment frames with reduced web section (RWS) connections under fire conditions. The reduced web section is achieved by introducing openings in the web of the steel beams, adjacent to the joint, similar to those which exist in cellular beams. RWS connections were initially devised in the 1990's for use in steel framed buildings in regions susceptible to seismic events, after it was observed that the common arrangement for fully fixed connections led to a brittle failure mode during earthquake events. For example, the Northridge earthquake of 1994 in Los Angles resulted in the brittle failure of fixed connections in steel moment frames in the zone where the beam flange was welded to the column face. This led to a weak, and un-ductile, performance of the connection and frame due to the formation of a plastic hinge in this critical area.

Following on from similar observations of brittle failures, different methods for strengthening fixed joints were proposed, including reinforcing the joint with externally bonded plates and effectively weakening the beam in line with the strong column/connection, weak beam principle. Researchers proposed a new type of joint, known as a reduced beam section (RBS) connection with the aim of moving the plastic hinge away from the column during seismic events thus delaying or preventing overall collapse. In RBS connections, the cross-sectional area of the beam is reduced at the beam ends by removing some of the top and bottom flanges (see Fig. 1(a), which is a schematic adapted from [1]). This reduces the plastic moment capacity in these regions and moves the critical section away from the column to the reduced beam section, thereby increasing the ductility of the connection.

Studies have demonstrated that the amount of material reduction in the flanges as well as the distance between the reduced section to the column edge are influential to the ductility and strength of the frames [2]. Engelhardt et al. [3] showed that reducing the flange width by more than 40–50 % compared with the original cross-section is likely to cause beam stability problems such as web buckling, torsional buckling, and local buckling in the compression flange. More studies have been conducted to understand the influence of floor slabs on the behaviour [4] as well as the effect of panel zone strength ratio on RBS connections [5]. While RBS connections certainly improve the overall survivability of steel moment frames during an earthquake, they also have some disadvantages. They can lead to the beam being susceptible to lateral torsional buckling failure, which ultimately leads to extensive strength degradation in the joint. The reduced portion of the flange to support the

* Corresponding author.
E-mail addresses: k.cashell@ucl.ac.uk (K.A. Cashell), mikko.malaska@tuni.fi (M. Malaska).

https://doi.org/10.1016/j.jcsr.2025.109938
Received 6 June 2025; Received in revised form 30 August 2025; Accepted 1 September 2025
Available online 13 September 2025

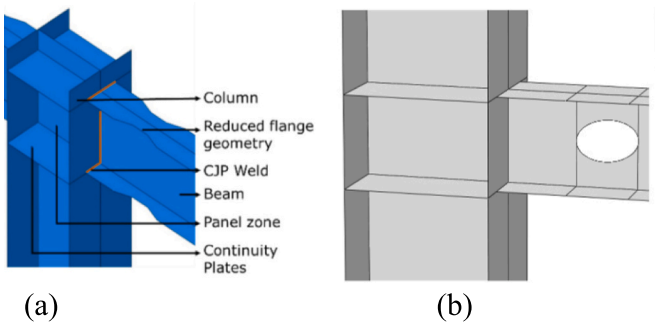

Fig. 1. Schematic view of (a) a typical RBS connection [1] and (b) a RWS connection.

web can result in local web buckling and also there can be some column twisting in deep column connections as a result of lateral torsional buckling of the beam.

In this context, an alternative "beam weakening" strategy is to employ a reduced web section (RWS) connection, as shown in Fig. 1(b). In these, the web area is reduced by cutting an opening such as those found in cellular beams. RWS connections have been the subject of much fewer research studies compared with RBS connections, although more information been made available in recent years. Different opening arrangements have been examined including introducing two parallel slots on the beam web [6], as well as rectangular [7] and circular [8] openings. It was shown that all of these reduce the stress concentrations in the connection, leading to ductile behaviour, and also result in greater distance between the location of the plastic hinge, in the beam, and the column edge. Design procedures have been proposed [9] in accordance with AISC 358 [10]. Previous studies have shown that RWS connections can enhance lateral-torsional buckling resistance compared to plain beams, due to the redistribution of material and the resulting change in stiffness and moment gradient near the reduced section [11].

The current paper is concerned specifically with RWS moment connections under fire conditions, for which there is very little performance information available in the literature. Although the multi-hazard event of an earthquake, followed by a fire is of course also relevant to this, the current paper is concerned with single-hazard fire events only, albeit in structures designed for seismic regions. Fire is one of the key limit states for steel structures, owing to its high thermal conductivity, and typically high section factor (H_p/A where H_p is the perimeter of the section and A is the cross-sectional area). Usually, steel structures are designed to have fire protection, which is very expensive, to insulate the key areas from unacceptable levels of structural degradation during a fire. One of the key areas of a structure during an extreme event is the connections, and they may be required to undergo large deflections without failure in order to maintain overall structural stability and resistance. For this reason, connections have been subjected to significant scrutiny from the research community in recent years (e.g. [12,13]). Studies such as these have led to the development of numerical and analytical models (e.g. [14,15]).

The current paper proceeds with a detailed description and analysis of a new fire test which was conducted at Tampere University in Finland in collaboration with Brunel University London and University College London. The principal aims of test were to (i) develop a fundamental understanding the fire behaviour of these details, and (ii) provide sufficient data so that a numerical model could be validated and then used to conduct a wider study. Accordingly, the important data recorded during the test is presented, including the deflections, fire resistance in minutes, failure mode and temperature profile and gradient at key locations. This is followed by a description of the FE model that was developed, and validated using the test data. This is then employed to conduct a detailed study on the fire behaviour of RWS connections with different details.

2. Fire test on an RWS connection

A fire test was designed and conducted on a reduced web section (RWS) connection to assess how this type of a connection behaves under fire conditions. This was the first fire test of its type, and therefore the data is very important not only for observing the behaviour, but also for validating numerical and analytical models which can be used to explore many more variables and influential parameters.

2.1. Test specimen and arrangement

Fig. 2 presents a schematic diagram of the test setup in the furnace at Tampere University. It is observed that the joint specimen consisted of two identical welded connections forming a double-sided beam-to-column joint configuration. The vertical member was made using a HEB 160 structural section. Two horizontal beam members comprising IPE 140 structural sections, were welded to the column flanges with 6 mm filled welds. In the joint region, the cross-section of the horizontal I-sections was reduced by creating elliptical web openings. The vertical steel section was reinforced with 8 mm thick web stiffeners and 10 mm thick web doublers in order to ensure that failure occurred in the beam sections. These plate thicknesses were selected following some initial studies on the behaviour of the plates, in order to ensure buckling did not occur. All of the I-sections and 10 mm steel plates were made from grade S355J2 carbon steel, in accordance with EN 10025–2:2019 [16], while the 8 mm plates were made using grade S355MC carbon steel, in accordance with EN 10149–2:2013 [17].

The testing furnace had a rectangular chamber with internal dimensions of 3000 mm × 3000 mm × 4000 mm (height × width × length). The specimen's vertical member was bolted to a steel loading frame located above the furnace, so the joint specimen hung from the frame; see Fig. 3(a) for a photographic image of the arrangement. An end plate of 400 mm × 300 mm × 20 mm (length × width × thickness) was welded to the end of the HEB 160 member, and the plate was fixed to the frame above the furnace with four bolts. The joint was loaded using two hydraulic loading jacks fixed to the loading frame, as shown in Fig. 3(b). Two long steel plates (1470 mm × 220 mm × 10 mm) were welded to the ends of the horizontal members and bolted to the hydraulic loading jacks located above the furnace roof. These plates served primarily to transfer tensile load from the jacks to the specimen and to maintain alignment during testing. While they were not designed to provide full rotational restraint, they did offer some resistance to out-of-plane displacement and helped stabilise the beam ends during heating. The 10 mm thickness was sufficient for these purposes, particularly as the plates were fire-protected to prevent thermal degradation. This setup ensured consistent load application while allowing for realistic thermal and mechanical boundary conditions.

2.2. Instrumentation

Although only one physical test was conducted due to the complexity and cost of full-scale fire testing, several measures were taken to ensure the reliability and reproducibility of the results. These include the use of consistent material properties verified through tensile coupon tests, detailed instrumentation to capture temperature and displacement data, and the development of a validated finite element model to extend the findings beyond the single test case. The joint specimen was heavily instrumented during the test, with thermocouples and linear variable differential transducers (LVDTs) to measure temperatures, displacements and deformations, see Fig. 4(b). The data from these devices was essential for the later validation of the numerical model. The steel temperatures were measured using 31 thermocouples installed in predrilled holes in the steel sections. The displacements of the horizontal beam stub ends were measured and monitored by the jacks located outside the furnace. In addition, joint deformations were measured using wires and steel screws fixed to the top flange of the IPE sections in

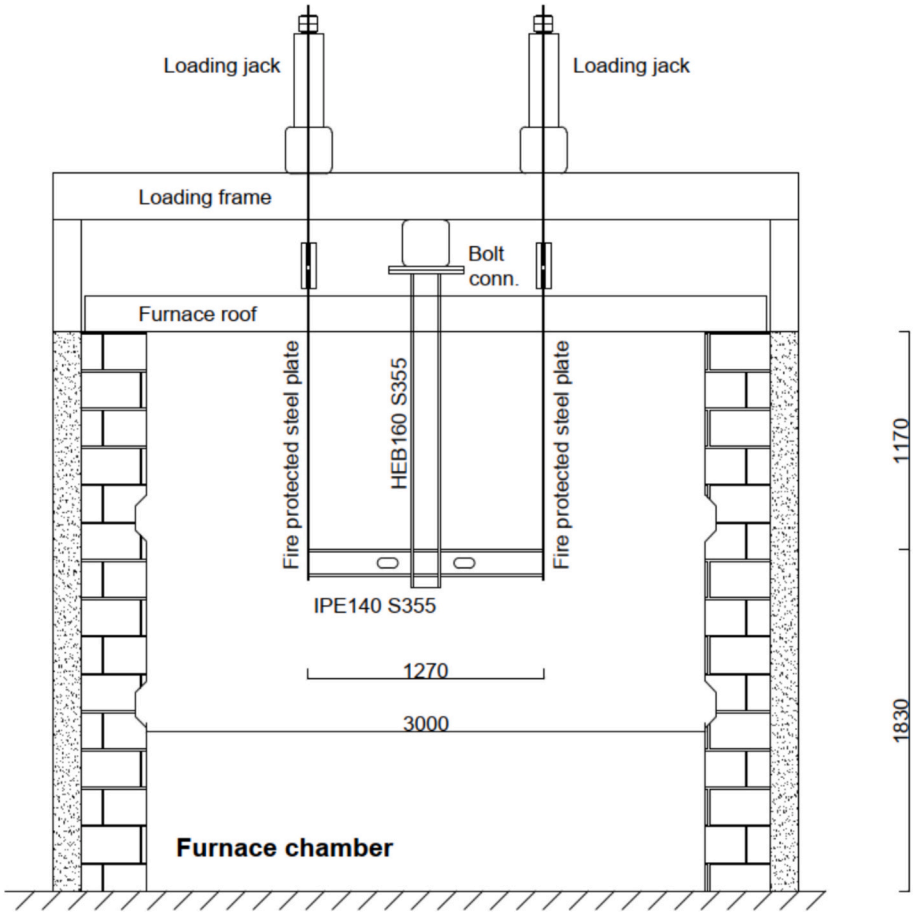

Fig. 2. A vertical cross-section of the test furnace and schematic of the experimental setup.

6 different locations. A molybdenum wire was attached to a steel screw, and pulled through two fixed pulleys outside the furnace and connected to a LVDT. The pulleys changed the direction of the molybdenum wire, and a 1 kg weight tied at the end kept the wire straight during the experiment. The elongation of the wire during heating was considered and eliminated from the measured displacements using a reference wire.

2.3. Material data

Tensile coupon tests were carried out in order to determine the mechanical properties at ambient temperature. The test pieces were prepared from the same batch of steel members as the tested joints, as shown in Fig. 5, and the tests were conducted in accordance with SFS EN 10002–1:2002 [18]. Three test pieces were flame-cut from the beam flange and web in the longitudinal direction of the IPE and HEB sections. Three pieces were also cut from the 8 mm and 12 mm thick steel plates that were employed in the joint configuration. The strains were calculated from the extension measurements using an extensometer over a gauge length of 50 mm. The average values for each of the measured steel material properties are listed in Table 1, where E, f_y and f_u are the Youngs modulus, yield strength and ultimate tensile strength, respectively, and ε_u is the ultimate strain.

2.4. Test procedure

The experimental fire test was divided into two phases. In the first phase, the specimen was loaded with the target axial force until the joint was stable. The target axial force was selected as approximately 25 % of the joint's bending moment resistance at ambient temperature, which was calculated using the material properties obtained from tensile coupon tests conducted on samples cut from the same batch of steel as the test specimen. These tests, performed in accordance with SFS EN 10002–1:2002 [18], provided accurate values for yield strength, ultimate strength, and Young's modulus, which were then used in conjunction with EN 1993-1-8 [19] to determine the joint's design moment capacity. In the second phase, the specimen was exposed to an ISO-834 standard fire until failure, after which the temperature reduced to ambient at a natural rate. For the applied axial force, two identical forces were applied to the IPE beam stub members through loading jacks and the long steel plates welded to the stubs. These forces resulted in a combined shear force and bending moment acting on the beam-to-column joints. The applied axial loading was kept constant throughout the test. The design bending moment resistance was calculated according to EN 1993-1-8 [19] using the steel material properties determined in tensile coupon tests described previously. Accordingly, the estimated joint bending moment resistance was 24 kNm and the corresponding applied jack loading was 20 kN per jack.

2.5. Test results

Fig. 6 presents the target standard time versus temperature response, in accordance with ISO 834 [20], together with the measured values during the test through the cross-section of the specimen and in the furnace. It is clear that the furnace temperature was very well matched with the target fire curve. As expected, the temperatures in the specimen were somewhat lower at each time point, but the differences between the furnace temperatures and the specimen temperatures reduced as the fire progressed. The results show that the temperatures at different locations of the IPE cross-section were uniform.

The test was terminated and the burners were switched off 16.5 min

(a)

(b)

Fig. 3. Test furnace arrangements including (a) a photographic image of the specimen inside the furnace before testing and (b) the loading frame and jacks outside of the furnace.

after the commencement of the test as the displacements began to increase significantly and very quickly, as shown in Fig. 7. The end displacements of the IPE beam stub members (as measured by LVDTs 7 and 8) and the local joint displacements at the end of the web opening (LVDTs 1 and 6) are presented in Fig. 7. The four curves show very similar shape, with very low levels of deflection developing until around 14 min into the fire, when the deflections increased rapidly, indicating that the joint was beginning to fail. A deflection limit of L/20 was used as the failure criterion, corresponding to a threshold of 28 mm. The displacement measured by LVDT 7 exceeded this value at 15 min and 40 s. The test results indicate a rapid increase in deflection beyond this point, suggesting a loss of stiffness ans validating the use of L/20 as an appropriate failure criterion. The measured displacements of the other LVDTs (LVDTs 2–5) were considered insignificant because they remained below 1 mm throughout the duration of the test. These values were substantially lower than those recorded at the beam ends and near the web opening (LVDTs 1, 6, 7, and 8), which exhibited pronounced deformation and were therefore used for model validation and analysis. After 15 min of heating, when the specimen began to fail, the web and flange temperatures at the opening were 703 °C and 692 °C, respectively. The failure mode observed in the test was a Vierendeel mechanism at the opening, as shown in Fig. 8.

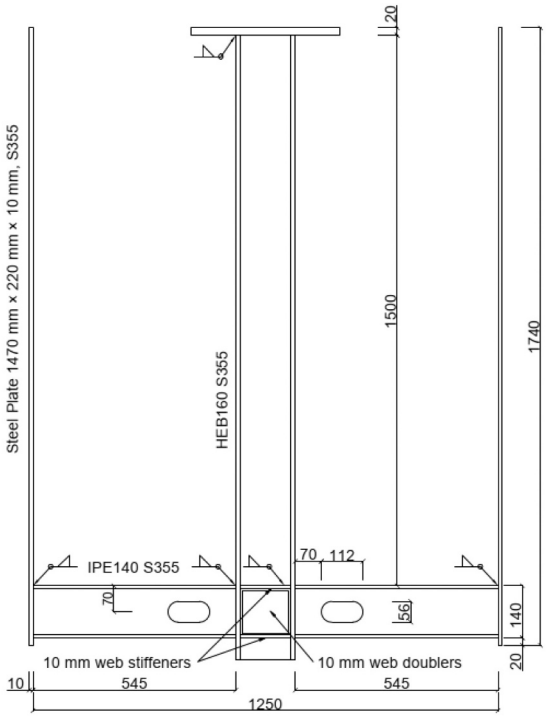

(a)

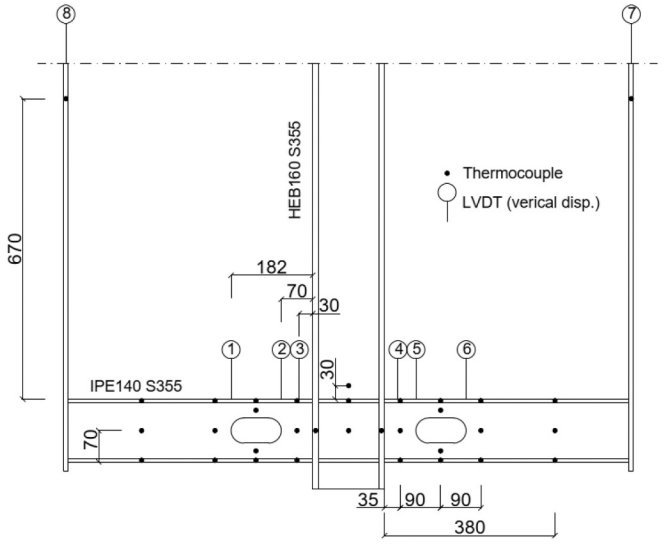

(b)

Fig. 4. (a) Specimen design and (b) instrumentation details.

Figs. 9–11 present a more detailed view of the change in temperatures, with time, at various key locations in the beams, column and beam-to-column interface. Firstly, Fig. 9 presents the variation in temperature measured by the thermocouples located along the top flanges of the beam members. It is clear that the temperatures did not rise quite as rapidly for the thermocouples located near the column face, as some protection was offered in this location. Otherwise, the temperatures were quite consistent along the beam. A similar phenomenon is also visible in Fig. 10 which presents corresponding data at locations in the web near the opening; the results from the thermocouples in the bottom flange are not presented here for brevity but are similar. As before, the thermocouples closest to the column face measured the lowest

Fig. 5. Steel sections and plates from which the test coupons were cut for material testing.

Table 1
Mechanical properties of the steel components (average values and standard deviations).

Profile		ε_u	f_y	E	f_u
		%	N/mm^2	kN/mm^2	N/mm^2
IPE140	**Web**	24.3	458 ± 24	208 ± 1	538 ± 5
	Flange	23.6	401 ± 30	206 ± 2	540 ± 6
HEB160	**Web**	20.8	462 ± 15	207 ± 4	555 ± 3
	Flange	23.8	446 ± 9	206 ± 1	538 ± 4
10 mm plate		22.4	553 ± 1	203 ± 3	584 ± 2
8 mm plate		19.1	467 ± 2	227 ± 6	546 ± 3

temperatures and also took longer to increase in temperature, compared with the other web/flange locations.

It is interesting to note through comparison between all of the data presented in Figs. 9 and 10, that the peak temperatures of just over 700 °C were similar in value at the web and top flanges and were also measured in all locations, at almost identical times (around 16.5 min after the test began); this was also observed in the bottom flanges. This indicates that all locations in the steel beam are vulnerable to rapid elevated temperature spread through the section. Fig. 11 presents the elevated temperature versus time data at locations at the beam to column interface, including the various stiffener and doubler plates as required for seismic design. In this case, the web doubler plate was the slowest component to reach each level of elevated temperature, most likely owing to its orientation relative to the application of temperature and the greater concentration of steel in the joint area.

3. Development of the numerical model

A finite element numerical model was developed in order to further understand the key behavioural aspects of RWS connections in fire. The model was developed in the Abaqus software [21] and then validated using the test results previously described. The numerical model was capable of capturing both the geometrically and materially nonlinear behaviour of reduced web section connections in fire conditions.

3.1. General details

The RWS connection was modelled using shell elements known as S4RT in the Abaqus library. The S4RT shell element was used to define both the beam and column components and it is a 4-noded, thermally-coupled, doubly-curved element, with reduced integration and finite membrane strains. This approach balances computational efficiency with accuracy and helps mitigate shear locking effects, particularly in regions dominated by bending. The element has four corner nodes, each with six degrees of freedom, and is suitable for either thick or thin shell applications. The model was first developed based on the test details as previously described, as the results are employed for validation of the approach.

A mesh sensitivity study was performed to identify an appropriate mesh density to achieve suitably accurate results whilst maintaining computational efficiency. Following this, the meshing of the numerical

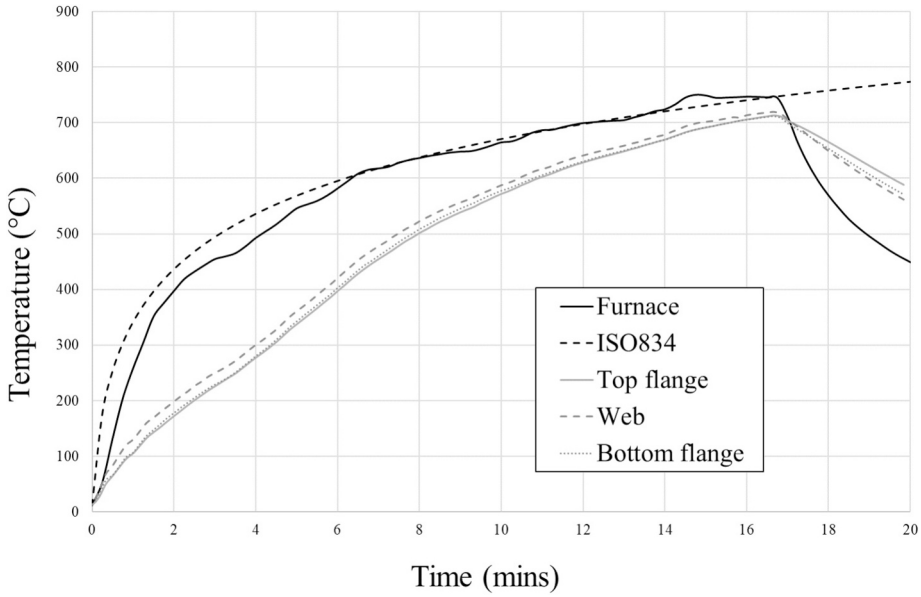

Fig. 6. Measured furnace and steel beam temperatures at the vicinity of the web opening.

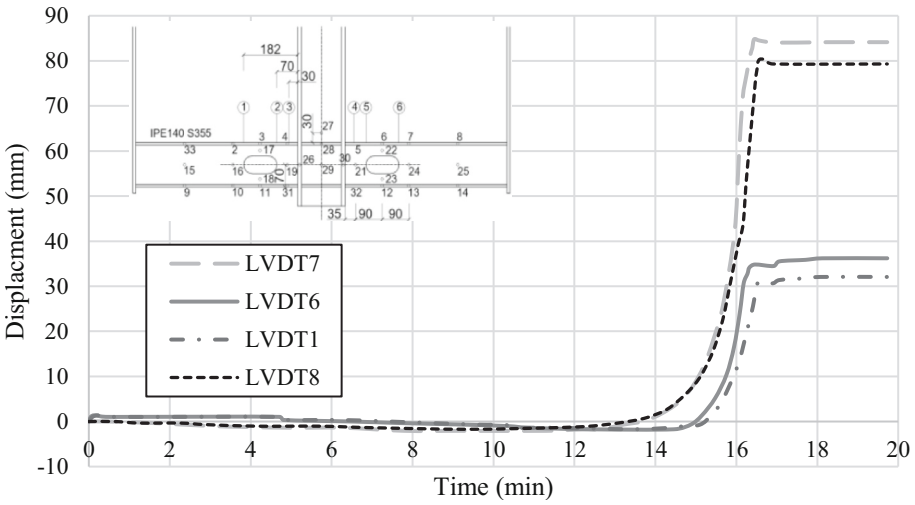

Fig. 7. Development of displacement at different locations in the beam versus time.

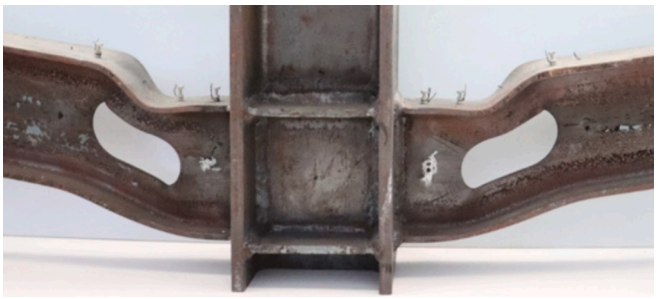

Fig. 8. Deformed RWS connection after the fire test.

model is specified by sweep technique and a mesh size of 15 mm for the region near the connection and 20 mm for the other areas was employed. The analysis was run as a mechanical-thermal two-stage process, similar to the fire test. Accordingly, an initial mechanical load was first applied and then the connection was subjected to elevated temperature, based on the time-temperature response during the testing programme. The thermo-mechanical analysis was conducted using a nonlinear, incremental, and iterative solution scheme. Automatic time stepping was employed with a minimum increment of 0.1 s and a maximum of 10 s. Convergence was assessed using both force and displacement norms, with tolerances set to 1 % to ensure numerical stability and accuracy throughout the simulation.

3.2. *Material properties*

The ambient temperature material properties, as given in Table 1, were employed to represent the steel stress-strain response in the model. At elevated temperature, the reduction factors as given in Eurocode 3 Part 1–2 [22] were employed to represent how each of the key mechanical characteristics such as 0.2 % proof strength, ultimate strength, ultimate strain and the elastic modulus, vary at different levels of elevated temperature. The model also adopted the coefficient of thermal expansion, the specific heat and the thermal conductivity for carbon steel based on the guidance given in Eurocode 3 Part 1–2 [22]. According to Eurocode 3 Part 1–2, the surface emissivity for carbon steel is considered to be 0.7, and the convective heat transfer coefficient of 25 W/m^2K; these values were employed in the FE analysis [23]. It is noteworthy that the material properties used in the numerical model were defined using true stress–strain relationships. These were obtained by converting the nominal stress–strain data from elevated temperature

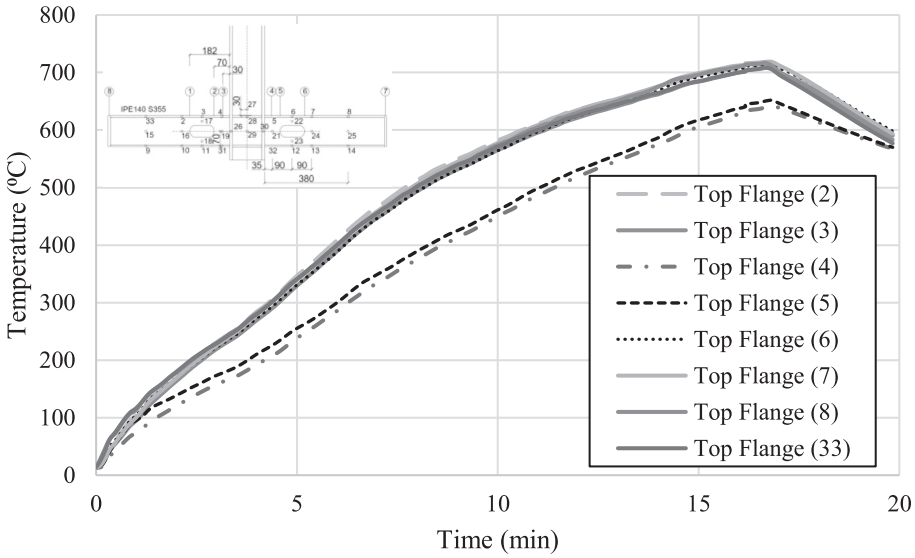

Fig. 9. Temperature versus time at various locations along the beams top flanges.

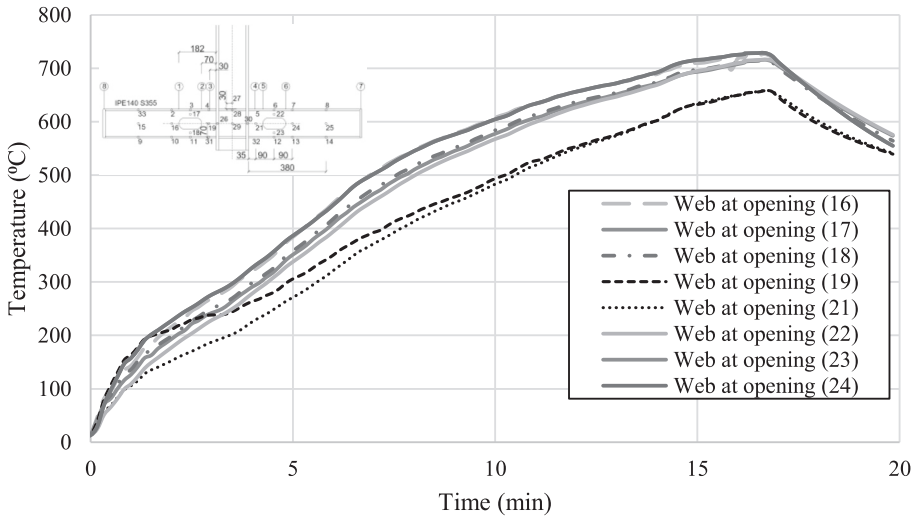

Fig. 10. Temperature versus time at various locations in the web, near the opening.

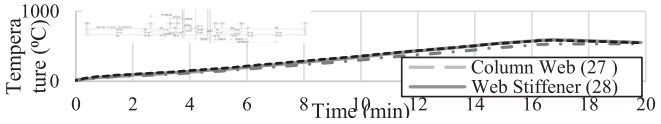

Fig. 11. Temperature versus time at various locations in the beam/column region.

data taken from the literature [22–24] using standard relationships that account for large deformation effects. This ensured that the material response under significant thermal and mechanical strain was accurately represented in the simulations.

3.3. Boundary and loading conditions

The boundary and loading conditions of the connection were modelled to simulate the exact conditions of the test specimen discussed previously this paper. Accordingly, two identical concentrated forces equal to 20 kN each were applied to the ends of the IPE 140 beam members. The self-weight of the elements was taken into account in the simulation. This was maintained at a constant value until the joint was stable. Then, the heat was applied in accordance with an ISO 834 standard fire and a coupled temperature-displacement analysis was performed. For the boundary conditions, the displacement at the top of the column was restrained in all directions, as shown in Fig. 12. To implement the experimental boundary condition in the finite element model, the ends of the horizontal beam members were constrained such that all rotational degrees of freedom (about the x, y, and z axes) were restricted while allowing vertical translation (along the global z-axis). This was achieved by applying boundary conditions to reference points at the beam ends, connected via rigid links to the beam nodes, ensuring that the ends could displace vertically but remained rotationally fixed. This setup replicates the experimental condition where the beam ends were bolted to vertically movable, but rotationally restrained, loading plates.

3.4. Validation

The finite element model was validated against the experimental results from the single test specimen. Despite the limitation of having only one physical test, the model accurately reproduced the observed behaviour, including temperature profiles, displacement histories, and failure modes. This validated model was then used to conduct a comprehensive parametric study, thereby enhancing the

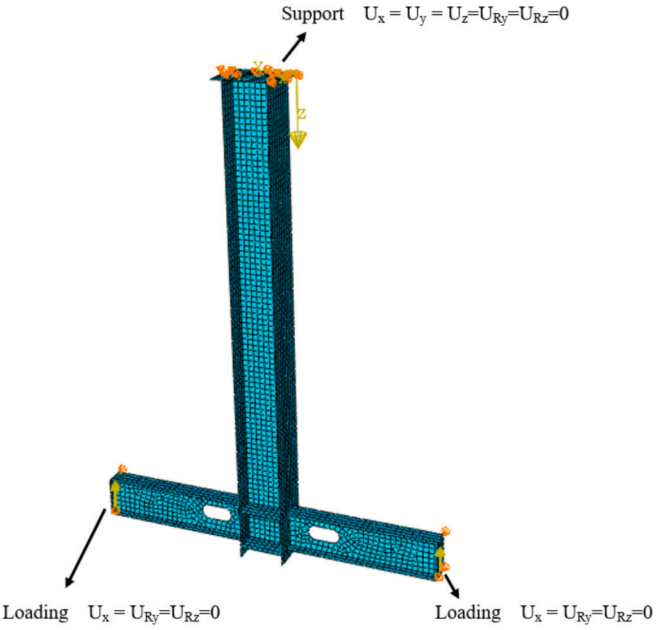

Fig. 12. Image from the FE model illustrating loading and boundary conditions.

generalizability and robustness of the findings. In addition, it is noteworthy that the default values for parameters in the thermal analysis (e.g. Boltzmann constant, absolute zero temperature) are adopted in accordance with the default values given in ABAQUS.

Fig. 13 presents the deflection versus temperature response obtained during the physical experiment together with the corresponding values predicted by the finite element model. The results are compared for the joint displacements at the end of the web opening (represented by LVDT 6 in the test) and also for the end displacements of the beam members (as measured by LVDT 7). To determine the accuracy of the FE model in comparison with the experiment, the RMSE (Root Mean Square Error) and corresponding R^2 values for the data from LVDT 7 were calculated and had values of 4.03 and 0.99, respectively. This is presented in Fig. 14.

It is clear from the data presented that the FE model provides a realistic response compared with the experimental values. The response can be generally divided into two phases. First, up to a temperature of

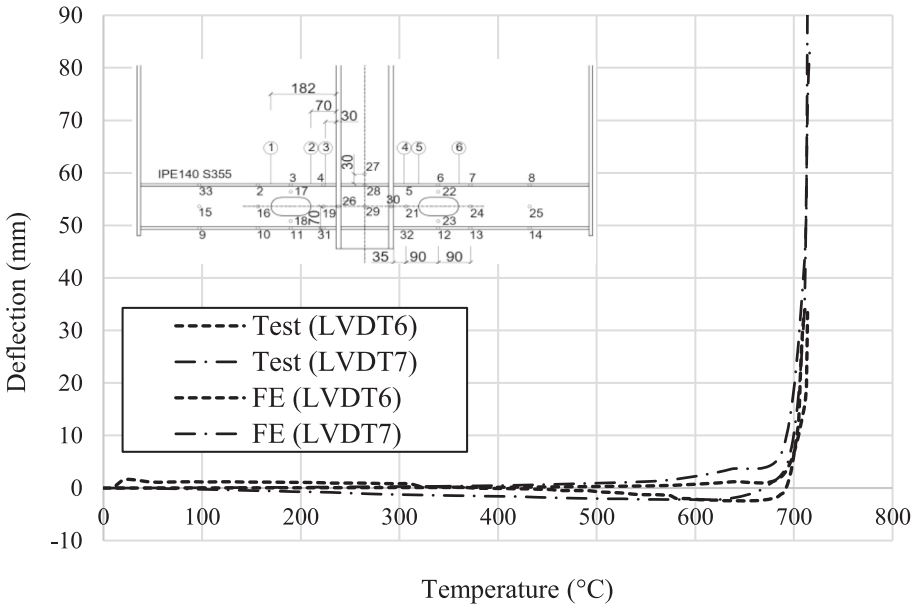

Fig. 13. Deflection versus temperature response for the experiment and numerical model for the RWS connection at the web opening (LVDT6 in the test) and beam end (LVDT7 in the test).

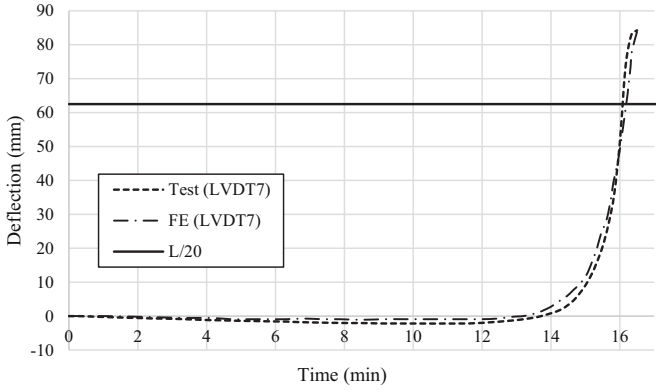

Fig. 14. Development of deflection versus time at LVDT 7) in the experiment.

around 680 °C, there were very low levels of deflection owing to the absence of any horizontal resistance to the development of thermal expansion. Then, once the temperature increased beyond 700 °C, the behaviour of the connection entered the second phase and the deflections suddenly increased significantly. At this temperature, there was a significant reduction in both the strength and stiffness of the steel material. The concentration of stresses at the corners of the web openings lead to buckling in the flanges directly above the opening, resulting in failure. These phenomena, which were observed in the test data, were very well replicated by the FE model.

In addition, the Von Mises stress distribution and deformations obtained from the finite element model were compared with the corresponding behaviour during the experiment. As shown in Fig. 15(a), the locations of the maximum Von Mises stresses in the finite element simulation, represented by the red/orange colours in the figure, correspond well with the location of significant deformations in the experimental specimen. In addition to the stress contour, a temperature distribution is shown at minute 16 in Fig. 15(b). It is clear that the overall deflected shape is accurately depicted, in particular in the region of the web openings. Overall, from the comparisons presented between the experimental and numerical results, it is concluded that the finite element model is capable of providing an accurate depiction of the RWS behaviour in fire.

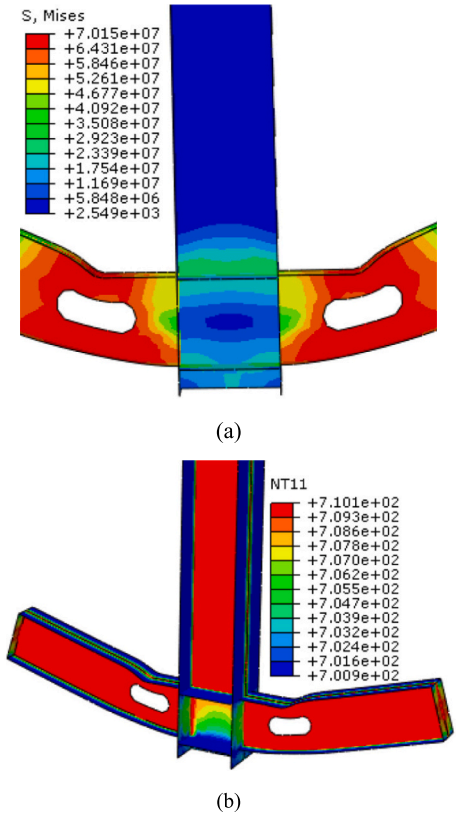

Fig. 15. (a) Deflected specimen from the numerical model illustrating the Von Mises stress distribution and (units: N/m^2) and (b) Temperature results (°C) from thermal model at $t = 16$ min.

4. Analysis of the behaviour of RWS connections in fire

In this section, the validated numerical model is used for an in-depth assessment and parametric study of RWS connections under fire conditions. The steel beams analysed in the parametric studies are designed to form a plastic hinge at a specified distance from the column. According

to the American Institute of Steel Construction (AISC) recommendations, this distance is proportional to the depth of the beam. In the current section, an IPE 360 beam section is selected to examine the effects of opening properties on the response. This differs from the laboratory test, which used an IPE 140 beam section designed in accordance with Eurocode 3 Part 1–2 [22], with loadings as given in Eurocode 1 Part 1–2 [25]. The IPE 140 section was selected owing to the loading and geometric limitations of the laboratory. On the other hand, in the current analysis, the IPE 360 with a length of 4000 mm, is selected as it is considered to be more realistic of a real application. The mechanical properties of the IPE 360 beam section, including elastic modulus, ultimate strength and yield strength are presented in Table 2. These properties are identical to those of the IPE 140 laboratory beam sample (see Table 1). Additionally, the material model used in the validated simulations in Section 3.2 are consistent with those employed herein. The locations of the loading and support points on the IPE 360 beam are illustrated in Fig. 16, while Fig. 17 and Table 5 provide geometric variables and specifications. The applied load on the beam in the midspan is 120 kN.

The study evaluates the impact of steel grade and load ratio on the connection's behaviour, as outlined in Table 2, while the geometric properties of the web openings are detailed in Table 5. All analyses consider the RWS connections exposed to a standard fire, with a heat transfer analysis performed to estimate temperatures at various points in the connection. The critical failure temperature is assumed to be uniform throughout the entire beam element.

While it is acknowledged that the standard fire is not necessarily representative of real fire scenarios, it is used here to replicate the experimental setup. The effects of different fire conditions will be investigated in future studies, which are beyond the scope of this work. As shown in Table 3, two load ratios (0.3 and 0.5) and four types of steel—carbon steel (CS), ferritic stainless steel (FS), austenitic stainless steel (AS), and duplex stainless steel (DS)—are analysed. The specific opening configurations will be discussed later.

4.1. Steel grade

This section compares the response of RWS connections made from four different metallic materials: carbon steel (CS), austenitic stainless steel (AS), ferritic stainless steel (FS), and duplex stainless steel (DS). Material properties significantly influence structural behaviour at ambient temperatures, with stainless steel generally exhibiting greater ductility than carbon steel. These differences are further pronounced at elevated temperatures due to variations in strength, stiffness, and ductility. The materials and their grades chosen are based on Cashell et al. (2021) and Arrayago et al. (2015) [23,24]. The ambient constitutive relationships for each material are selected based on data from Eurocode 3 Part 1–1 [19]. Key mechanical properties, including Young's modulus (E), yield strength (σ_y, defined as the 0.2 % proof strength for stainless steel, $\sigma_{0.2}$), ultimate tensile strength (σ_u), and ultimate strain (ε_u), are summarized in Table 4 [23]. The specific grades studied are SS400 for carbon steel, grade 1.4406 for austenitic stainless steel, grade 1.4477 for duplex stainless steel, and grade 1.4521 for ferritic stainless steel. Notably, both the austenitic and duplex stainless steels have significantly higher ultimate strains compared to the carbon steel. In addition, austenitic stainless steel exhibits not only high ductility but also significant strain hardening capacity, which contributes to its superior performance at elevated temperatures.

Table 2
Mechanical properties of the IPE 360 beam section.

	Elastic Modulus (GPa)	Ultimate Strength (MPa)	Yield Strength (MPa)
Flange	206	540	401
Web	208	538	458

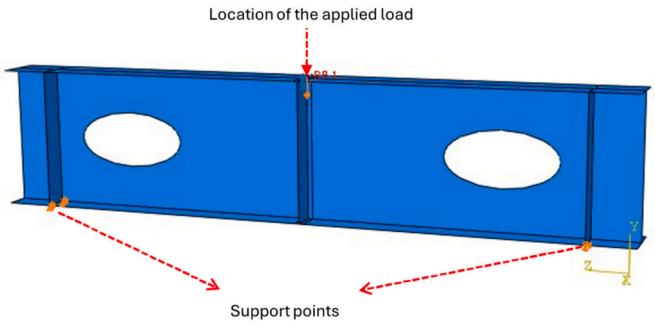

Fig. 16. IPE 360 beam with a reduced web-section (RWS).

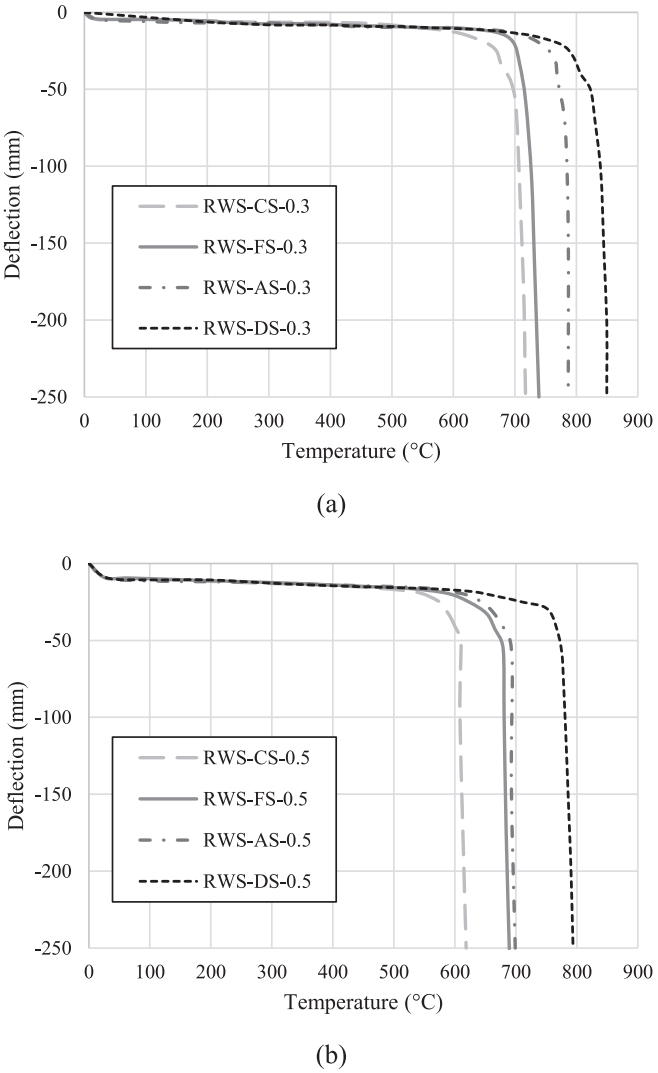

Fig. 17. Deflection versus temperature for beams made from various materials, for load ratios (a) 0.3 and (b) 0.5.

It is noted that sensitivity to load level varies not only between material types but also between grades within the same category. For example, among austenitic stainless steels, grade 1.4571 has been shown to exhibit greater sensitivity to load-induced degradation than grade 1.4301, due to differences in alloy composition and strain-hardening behaviour. While this study focused on grade 1.4406, future work should investigate such intra-category variations to refine fire design recommendations.

Table 3
RWS joints examined in the parametric study.

Model	Material type	Load ratio
RWS-CS-0.3	Carbon steel	0.3
RWS-FS-0.3	Ferritic stainless steel	0.3
RWS-AS-0.3	Austenitic stainless steel	0.3
RWS-DS-0.3	Duplex stainless steel	0.3
RWS-CS-0.5	Carbon steel	0.5
RWS-FS-0.5	Ferritic stainless steel	0.5
RWS-AS-0.5	Austenitic stainless steel	0.5
RWS-DS-0.5	Duplex stainless steel	0.5

Table 4
Mechanical specifications of elastoplastic material models [23].

Material type	E (MPa)	σ_y (MPa)	σ_u (GPa)	ε_u (%)
Carbon steel (CS)	206,000	400	540	20
Ferritic stainless steel (FS)	213,000	324	520	28
Austenitic stainless steel (AS)	203,000	302	653	67
Duplex stainless steel (DS)	209,000	652	854	41

Table 5
Details of geometric variables for the reduced cross-section area of the RWS connection with elliptical cut.

Model	a (mm)	b (mm)	h (mm)	d (mm)
Series A				
RWS-0.2-0.8-0.4	72	288	144	360
RWS-0.3-0.8-0.4	108	288	144	360
RWS-0.4-0.8-0.4	144	288	144	360
RWS-0.5-0.8-0.4	180	288	144	360
RWS-0.6-0.8-0.4	216	288	144	360
Series B				
RWS-0.4-0.5-0.4	144	180	144	360
RWS-0.4-0.6-0.4	144	216	144	360
RWS-0.4-0.7-0.4	144	252	144	360
RWS-0.4-0.8-0.4	144	288	144	360
RWS-0.4-0.9-0.4	144	324	144	360
Series C				
RWS-0.4-0.8-0.2	144	288	72	360
RWS-0.4-0.8-0.3	144	288	108	360
RWS-0.4-0.8-0.4	144	288	144	360
RWS-0.4-0.8-0.5	144	288	180	360
RWS-0.4-0.8-0.6	144	288	216	360

Table 6
Failure criteria for beams in bending according to BS 476.

Cross-Section	L (mm)	d (mm)	L/20 (mm)	L/30 (mm)	$L^2/(9000d)$ (mm/min)
IPE360	4000	360	200	133.3	4.94

Fig. 17 compares the deflection versus temperature of RWS connections subjected to a standard fire at load ratios of (a) 0.3 and (b) 0.5. This deflection has been recorded in the mid-span of the mid-height of the section. The results show that, for both load ratios, beams made from duplex stainless steel exhibit the highest fire resistance among the four materials tested, followed by austenitic stainless steel, ferritic stainless steel, and then carbon steel which was the first to fail. A closer analysis of the graph in Fig. 17 indicates that when the load ratio increases from 0.3 to 0.5, the difference in fire resistance between austenitic and ferritic stainless steel becomes negligible. Although austenitic stainless steels generally retain mechanical properties better at elevated temperatures, the specific ferritic grade used in this study (1.4521) demonstrated comparable fire resistance under the higher load ratio. This may be attributed to its relatively high yield strength and the influence of load-induced deformation, which can diminish the performance gap between the two grades. In contrast, carbon steel consistently shows the lowest performance in both load ratio scenarios. This is attributed to the lower sensitivity of austenitic stainless steel beams to deformation under load due to their high ductility. Based on these findings, it is reasonable to consider using stainless steel of any family examined here, including the more economic and price-stable ferritic grades, for RWS connections to achieve optimal fire resistance. Although it is not the focus of the current paper, this improved performance at elevated temperatures for the stainless steel connections, is in addition to what is likely to be a significantly better performance under seismic conditions.

4.2. Load ratio

Fig. 18 compares the bottom flange temperature versus mid-span vertical deflection for RWS beams made from the four different steel materials as before, considering two load ratios. The results indicate that the load ratio (LR) significantly impacts the fire behaviour of RWS connections, with fire resistance generally decreasing as the load ratio increases, regardless of steel grade or loading type. The results demonstrate that carbon steel and austenitic stainless steel RWS connections are more sensitive to changes in LR compared with duplex and ferritic stainless steel beams. Specifically, carbon steel and austenitic stainless steel show the largest reductions in fire resistance, at 14 % and 11 %, respectively. In contrast, the fire resistance of ferritic and duplex stainless steel decreases by approximately 6 % to 7 %. When the LR increases from 0.3 to 0.5, the fire resistance temperature drops by around 100 °C for carbon steel and 90 °C for austenitic stainless steel, while for ferritic and duplex stainless steel, the reduction is around 50 °C for both.

4.3. Opening properties

In the RWS designation for series A, B, and C, the first number represents the initial distance of the reduced area from the support as a proportion of the beam's depth, the second number indicates the length of the reduced area relative to the beam's depth, and the third number denotes its depth. For instance, model RWS-0.4-0.8-0.2 corresponds to a beam with an elliptical web cut where a = 0.4d, b = 0.8d, and h = 0.2d.

The models are analysed in three series. With reference to Fig. 19, in Series A, the elliptical cut length (b) and depth (h) remain constant, while the initial distance (a) varies. In Series B, a and h are fixed, and b changes; in Series C, a and b are constant, and h varies. The results in Fig. 20 compare steel beams with RWS connections across different reduced cross-section variables. These graphs reveal three distinct phases in the temperature-deflection response of the beam connections. Initially, deflections increase gradually and linearly with temperature. Around 650 °C, a sharp reduction in the material's mechanical properties causes a rapid increase in deflections and their rate of development. Beyond 700 °C, deflections continue increasing until failure occurs at approximately 250 mm.

Fig. 20(a) presents the increasing deflections at mid-span for beams with RWS connections with different a values, varying between 72 mm and 216 mm. The analysis shows that a beam with a = 72 mm is to a small degree, the most vulnerable during elevated temperature exposure, experiencing greater deformations at lower temperatures compared with the other arrangements. These deflection-temperature curves (Fig. 20(a)) indicate a significant deflection increase at approximately 650 °C, marking it as the critical failure temperature. At a mid-span vertical deflection of approximately 200 mm, the temperature for model RWS-0.2-0.8-0.4 is 705 °C, while other Series A models are around 715 °C. As deflection increases, the temperature difference between RWS-0.2-0.8-0.4 and the other models grows slightly, by less than 5 °C at 250 mm.

Series B examines the effect of varying the elliptical cut length (b) on fire resistance, as shown in Fig. 20(b). The results show that Series B

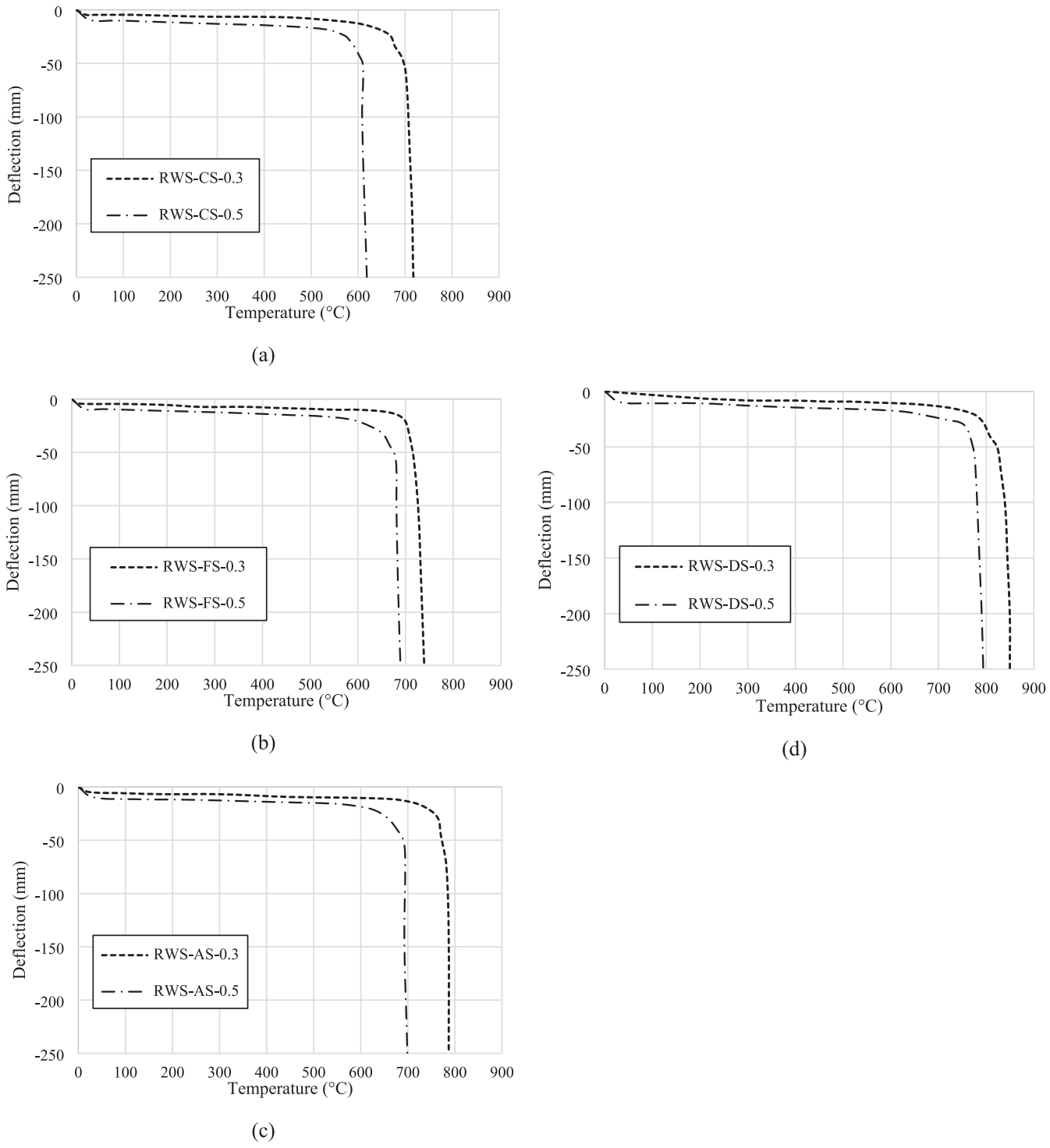

Fig. 18. Effect of load ratios on steel types for (a) CS, (b) FS, (c) AS and (d) DS.

models also experience a marked deflection increase at 650 °C. At deflections of around 200 mm, temperatures range from approximately 710 °C (RWS-0.4-0.9-0.4) to 720 °C (RWS-0.4-0.5-0.4). The analysis suggests that reducing b slightly improves fire resistance, although it is a marginal effect. Series C investigates the influence of the elliptical cut depth (h). As shown in Fig. 20(c), deflections again increase sharply at around 650 °C. At 200 mm deflection, temperatures range from approximately 710 °C (RWS-0.4-0.8-0.6) to 725 °C (RWS-0.4-0.8-0.2). The results indicate that reducing h does slightly enhance fire resistance, with temperature differences between models remaining minimal beyond 200 mm deflection. It is also noteworthy that although the mid-span deflection curves in Fig. 20(c) appear similar across different elliptical cut depths, a closer examination reveals that specimens with deeper cuts (e.g., 0.6d) experienced earlier failure and lower critical temperatures. This indicates that cut depth significantly influences fire resistance, not through peak deflection magnitude, but through the rate of deformation and time to failure.

Whilst RWS are not considered in design codes, BS 476 Parts 20 and 21 [26,27], provide failure criteria to define bending failure in solid steel connections (i.e. not RWS). It is assumed that the arrangement has

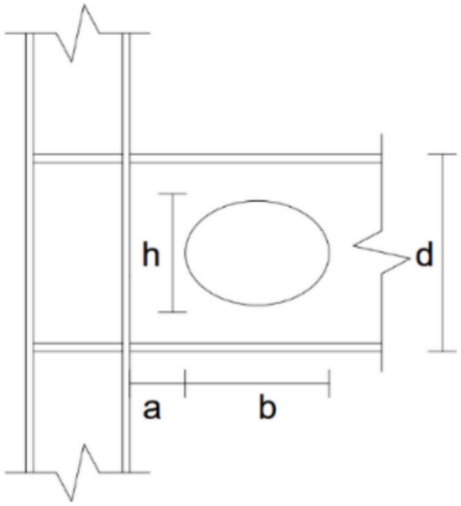

Fig. 19. Schematic view of the RWS connection and the geometric variables relating to the web opening.

failed if either of the following criteria are met: (1) if the beam deflection exceeds one-twentieth of its free span length (L), or (2) the deflection exceeds one-thirtieth of L, and the deflection rate surpasses $L^2/9000d$. Table 6 summarizes these criteria for the IPE 360 beam models. The results presented herein confirms that all IPE 360 beam models meet the first BS 476 failure condition, as deflections exceed 200 mm.

Variations in parameters such as the distance from the centre of the reduced area to the support (a) and the length of the reduced area (b) have minimal impact on the critical temperature of the beam, which remains around 650 °C. However, the elliptical cut depth (c) does influence the fire performance, with greater depths leading to lower critical temperatures. For instance, a beam with an elliptical cut depth of 0.2d has a critical temperature of approximately 685 °C, whereas increasing the depth to 0.6d reduces it to about 627 °C. This reduction is due to the corresponding decrease in cross-sectional area.

The analysis shows that fire resistance remains largely unchanged when the initial distance of the reduced area from the column (a) varies between 0.3d and 0.6d, indicating that a minimum distance of 0.3d is suitable for fire resistance design. As deflection increases, Series A models exhibit similar behaviour. While the elliptical cut length (b) has little impact on fire resistance, it may offer slight improvements. Likewise, although the elliptical cut depth (c) is not a dominant factor, it should be considered when optimising fire resistance in RWS beam connections.

5. Design implications for RWS connections in fire

Although RWS connections are not yet explicitly covered in major design codes, the findings from this study provide a foundation for developing practical design guidance. Based on the validated numerical model and parametric studies, the following quantitative recommendations are proposed:

- Critical temperature threshold: The onset of significant structural degradation consistently occurred around 650 °C, regardless of geometry or material. This value can be used as a conservative benchmark for fire design of RWS connections.
- Elliptical cut depth (h): The depth of the web opening has the most significant influence on fire resistance. To delay failure, it is recommended that $h \leq 0.4d$, where d is the beam depth. Deeper cuts (e.g., 0.6d) led to earlier failure at temperatures as low as 627 °C.
- Distance from column (a): The distance between the reduced section and the column face should be $a \geq 0.3d$. Increasing this distance beyond 0.4d had minimal additional benefit in terms of fire resistance.
- Material selection: Duplex stainless steel consistently outperformed other materials, maintaining structural integrity up to 850 °C. For critical connections in fire-prone or seismic regions, duplex stainless steel is recommended, followed by austenitic and ferritic stainless steels.
- Load ratio sensitivity: Fire resistance decreases with increasing load ratio. For carbon steel, increasing the load ratio from 0.3 to 0.5 reduced the critical temperature by approximately 100 °C. Designers should aim to limit the load ratio to ≤0.3 where possible.

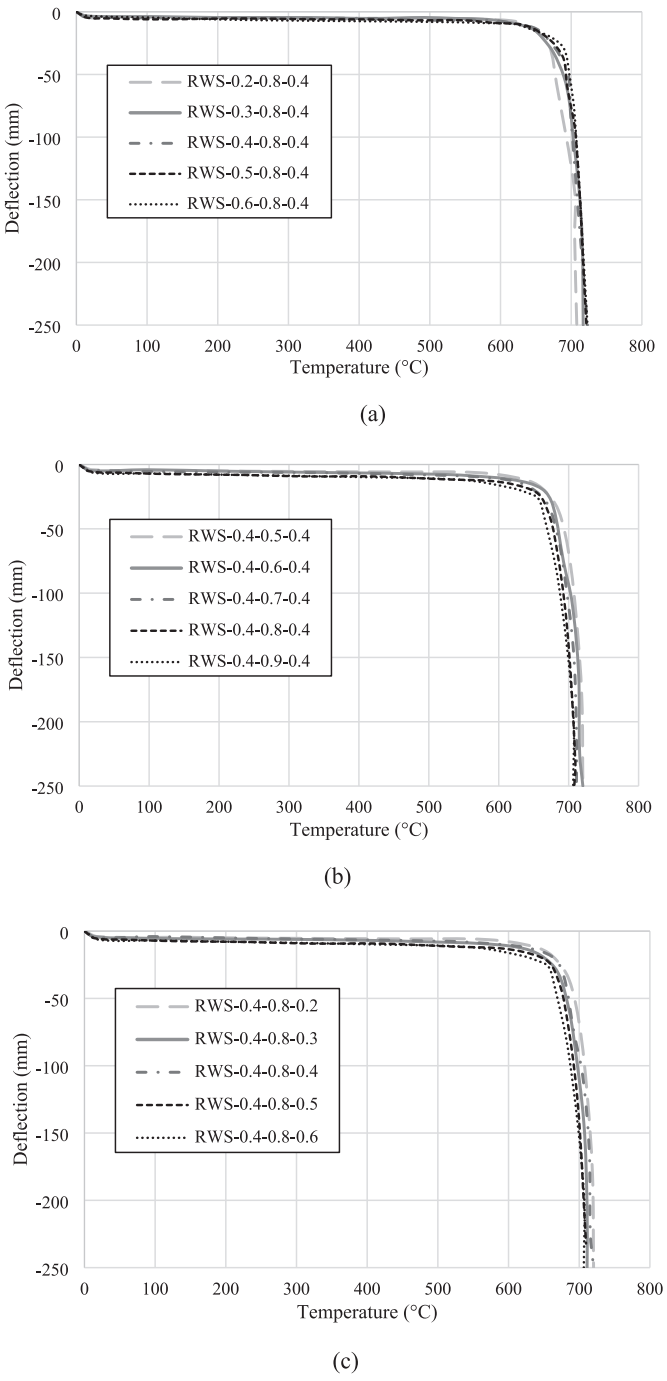

Fig. 20. Comparison of steel beams with RWS connections made from different reduced cross-section variables for (a) series A, (b) series B and (c) series C.

These findings can inform preliminary design checks and support the

development of simplified design rules for RWS connections under fire conditions. Future work should aim to integrate these recommendations into performance-based fire design frameworks and validate them against additional experimental data.

6. Conclusions

This paper presents an in-depth analysis of the fire behaviour of steel beams with reduced web section (RWS) connections. The first fire test on these arrangements is discussed in detail and the key results and observations are presented. A finite element model is also developed to supplement the fire test data, and is employed to understand the relative influence of key parameters such as steel grade, load ratio, and opening properties on the behaviour. The main conclusions from this research include:

1. The deflection-temperature of steel beams with RWS connections can be categorized into three distinct phases. A notable finding is that the critical temperature, where significant structural failure begins, is consistently around 650 °C for most models. However, the elliptical cut depth (c) has a relatively large effect on this critical temperature, with deeper cuts leading to lower critical temperatures and, consequently, earlier onset of structural failure.
2. The observed failure mechanism—characterised by vertical shear and localised bending at the web opening—is consistent with known Vierendeel-type behaviour, but this study provides the first detailed validation of this mechanism in RWS connections under fire conditions.
3. The progressive development of mid-span deflection and the associated temperature thresholds confirm the applicability of established fire design principles to RWS connections, while also highlighting the importance of local geometry in influencing failure timing.
4. It is noteworthy that the critical temperature of approximately 650 °C observed in the carbon steel RWS connection aligns with the limiting temperature specified in Eurocode EN 1993-1-2 for typical load levels. This consistency supports the applicability of existing fire design guidance to RWS connections and reinforces the reliability of the simulation results.
5. The results show that while the distance from the reduced area to the column (a) and the elliptical cut length (b) have minimal impact on the critical temperature, they do influence the overall fire resistance of the beam. Notably, the elliptical cut depth (c) has a significant effect, as deeper cuts lead to earlier failure. For optimal fire resistance, it is recommended to maintain a distance (a) of at least 0.3d and to carefully consider the depth of the elliptical cut.
6. Based on the findings, several recommendations are made for the fire design of steel beams with RWS connections. To enhance fire performance, it is recommended to prioritize the use of duplex stainless steel and consider limiting the elliptical cut depth. Additionally, maintaining a sufficient distance between the reduced area and the column is crucial for ensuring structural stability under fire conditions.

Overall, this research presented herein advances the understanding of RWS connections under fire conditions. Nevertheless, it is recommended that future research should explore the influence of different, more realistic fire scenarios and should also see to further refine the design recommendations for different structural configurations. In addition, while this study provides valuable insights into the fire performance of RWS connections, it is acknowledged that the experimental programme was limited to a single carbon steel specimen due to practical constraints. Future research should aim to include additional fire tests, particularly on stainless steel joints, to further validate and generalize the findings presented herein. Finally, given that RWS connections are generally employed in seismic zones, the influence of employing stainless steel for improved seismic behaviour should also be studied; this work is currently ongoing.

CRediT authorship contribution statement

Oday Yabari: Writing – original draft, Methodology, Investigation, Formal analysis, Data curation. **Katherine A. Cashell:** Writing – review & editing, Supervision, Project administration, Methodology, Funding acquisition, Formal analysis, Data curation, Conceptualization. **Mika Alanen:** Writing – original draft, Methodology, Investigation, Formal analysis, Data curation. **Mikko Malaska:** Writing – review & editing, Visualization, Validation, Supervision, Resources, Project administration, Methodology, Investigation, Formal analysis, Conceptualization.

Declaration of competing interest

The authors declare that they have no known competing financial interests or personal relationships that could have appeared to influence the work reported in this paper.

Acknowledgements

The authors gratefully acknowledge that the experimental work presented in this paper was supported through a Research England International Investment Initiative (I3) grant, awarded to Brunel University London with Tampere University as the international partner. The title of the award was “UK and Finland: Research collaboration for prosperity and health”.

Data availability

Data will be made available on request.

References

[1] S. Naimi, M. Celikag, A.A. Hedayat, Ductility enhancement of post-Northridge connections by multilongitudinal voids in the beam web, Sci. World J. 2013 (2013) 1–14, https://doi.org/10.1155/2013/515936.
[2] J. Shen, T. Kitjasateanphun, W. Srivanich, Seismic performance of steel moment frames with reduced beam sections, Eng. Struct. 22 (8) (2000) 968–983, https://doi.org/10.1016/s0141-0296(99)00048-6.
[3] Michael D. Engelhardt, Ted Winneberger, Andrew J. Zekany, Timothy J. Potyraj, Experimental investigation of Dogbone moment connections, Eng. J. 35 (1998) 128–139.
[4] S.L. Jones, G.T. Fry, M.D. Engelhardt, Experimental evaluation of cyclically loaded reduced beam section moment connections, J. Struct. Eng. 128 (4) (2002) 441–451, https://doi.org/10.1061/(asce)0733-9445(2002)128:4(441).
[5] A.A. Soliman, O.A. Ibrahim, A.M. Ibrahim, Effect of panel zone strength ratio on reduced beam section steel moment frame connections, Alex. Eng. J. 57 (4) (2018) 3523–3533, https://doi.org/10.1016/j.aej.2018.07.017.
[6] A.K. Swati, V. Gaurang, Study of steel moment connection with and without reduced beam section, Case Stud. Struct. Eng. 1 (2014) 26–31, https://doi.org/10.1016/j.csse.2014.04.001.
[7] A.A. Hedayat, M. Celikag, Post-northridge connection with modified beam end configuration to enhance strength and ductility, J. Constr. Steel Res. 65 (7) (2009) 1413–1430, https://doi.org/10.1016/j.jcsr.2009.03.007.
[8] M. Davarpanah, H. Ronagh, P. Memarzadeh, F. Behnamfar, Cyclic behaviour of elliptical-shaped reduced web section connection, Structures 24 (2020) 955–973, https://doi.org/10.1016/j.istruc.2020.02.016.
[9] K. Boushehri, K.D. Tsavdaridis, G. Cai, Seismic behaviour of RWS moment connections to deep columns with European sections, J. Constr. Steel Res. 161 (2019) 416–435, https://doi.org/10.1016/j.jcsr.2019.07.009.
[10] Seismic provisions for Structural Steel Buildings, ANSI/AISC 341–10, Structural Analysis and Design of Tall Buildings, 2011, pp. 355–410, https://doi.org/10.1201/b11248-8.
[11] M. Davarpanah, H. Ronagh, P. Memarzadeh, F. Behnamfar, Cyclic behaviour of elliptical-shaped reduced web section connection, Structures 24 (2020) 955–973, https://doi.org/10.1016/j.istruc.2020.02.016.
[12] X.H. Dai, Y.C. Wang, C.G. Bailey, An experimental study of structural behaviour of joints in restrained steel frames in fires, in: International conference, Application of Structural Fire Design, 2009, pp. 19–20. February 2009.
[13] K.D. Tsavdaridis, T. Papadopoulos, A Fe parametric study of RWS beam-to-column bolted connections with cellular beams, J. Constr. Steel Res. 116 (2016) 92–113, https://doi.org/10.1016/j.jcsr.2015.08.046.

[14] M. Davarpanah, H. Ronagh, P. Memarzadeh, F. Behnamfar, Cyclic behavior of welded elliptical-shaped RWS moment frame, J. Constr. Steel Res. 175 (2020) 106319, https://doi.org/10.1016/j.jcsr.2020.106319.
[15] A.A. Hedayat, M. Celikag, Post-northridge connection with modified beam end configuration to enhance strength and ductility, J. Constr. Steel Res. 65 (7) (2009) 1413–1430, https://doi.org/10.1016/j.jcsr.2009.03.007.
[16] EN 10025–-2, Hot rolled products of structural steels, Part 2: Technical delivery conditions for non-alloy structural steel, European Committee for Standardization (CEN), 2019, https://doi.org/10.3403/03152996.
[17] EN 10149–-2, Hot rolled flat products made of high yield strength steels for cold forming, Part 2: Technical delivery conditions for thermomechanically rolled steels, European Committee for Standardization (CEN), 2013, https://doi.org/10.3403/30239495.
[18] SFS EN 10002–-1, Metallic materials. tensile testing, Part 1: Method of test at ambient temperature, European Committee for Standardization (CEN), 2002, https://doi.org/10.3403/30144369.
[19] EN 1993-1-8, Eurocode 3: Design of Steel Structures, Part 1–8: Design of Joints, European Committee for Standardization (CEN), 2005, https://doi.org/10.1680/dgte3.31630.
[20] ISO 834-1:1999, Fire-resistance tests - Elements of building construction, Part 1: General requirements, International Organization for Standardization ISO 834, Geneva, Switzerland, 2021. https://iso.org/standard/81661.html.
[21] Abaqus/CAE User''s Guide, Dassault Systems. http://130.149.89.49:2080/v6.14/index.html, 2017.
[22] EN 1993-1-1-2 Eurocode 3: Design of Steel Structures, Part 1–2: General rules - Structural fire European Committee for Standardization (CEN).
[23] K.A. Cashell, M. Malaska, M. Khan, M. Alanen, K. Mela, Experimental and numerical analysis of stainless steel cellular beams in fire, Fire Saf. J. 121 (2021) 103277, https://doi.org/10.1016/j.firesaf.2021.103277.
[24] I. Arrayago, E. Real, L. Gardner, Description of stress-strain curves for stainless steel alloyd, Mater. Des. 87 (540) (2015) 552, https://doi.org/10.1016/j.matdes.2015.08.001.
[25] EN 1991-1-1-2. Eurocode 1: actions on structures. Part 1–2: General actions, Actions on structures exposed to fire, European Committee for Standardization, 2002. doi:10.3403/02700262.
[26] BS 476–-20. 1987 Fire tests on building materials and structures – Method for determination of the fire resistance of elements of construction (general principles), British Standards Institution, 1987.
[27] BS 476–-21. 1987 Fire tests on building materials and structures – Method for determination of the fire resistance of loadbearing elements of construction, British Standards Institution, 1987.